FULL PAPER

Structural and Electrochemical Study of Al$_2$O$_3$ and TiO$_2$ Coated Li$_{1.2}$Ni$_{0.13}$Mn$_{0.54}$Co$_{0.13}$O$_2$ Cathode Material Using ALD

Xiaofeng Zhang, Ilias Belharouak,* Li Li, Yu Lei, Jeffrey W. Elam, Anmin Nie, Xinqi Chen, Reza S. Yassar, and Richard L. Axelbaum

Nanolayers of Al$_2$O$_3$ and TiO$_2$ coatings were applied to lithium- and manganese-rich cathode powder Li$_{1.2}$Ni$_{0.13}$Mn$_{0.54}$Co$_{0.13}$O$_2$ using an atomic layer deposition (ALD) method. The ALD coatings exhibited different surface morphologies; the Al$_2$O$_3$ surface film appeared to be uniform and conformal, while the TiO$_2$ layers appeared as particulates across the material surface. In a Li-cell, the Al$_2$O$_3$ surface film was stable during repeated charge and discharge, and this improved the cell cycling stability, despite a high surface impedance. The TiO$_2$ layer was found to be more reactive with Li and formed a Li$_x$TiO$_2$ interface, which led to a slight increase in cell capacity. However, the repetitive insertion/extraction process for the Li$^+$ ions caused erosion of the surface protective TiO$_2$ film, which led to degradation in cell performance, particularly at high temperature. For cells comprised of the coated Li$_{1.2}$Ni$_{0.13}$Mn$_{0.54}$Co$_{0.13}$O$_2$ and an anode of meso-carbon-micro-beads (MCMB), the cycling stability introduced by ALD was not enough to overcome the electrochemical instability of MCMB graphite. Therefore, protection of the cathode materials by ALD Al$_2$O$_3$ or TiO$_2$ can address some of the capacity fading issues related to the Li-rich cathode at room temperature.

1. Introduction

Lithium-ion batteries (LIBs), which are commonly used in portable electronics, have shown a growing penetration in larger applications such as transportation.[1,2] For these applications, high durability, improved safety and high-energy densities are key requirements. Among the advanced cathode materials, lithium- and manganese-rich (LMR) oxides, xLi$_2$MnO$_3$·(1-x)LiMO$_2$ (M = Mn, Ni, and Co), are promising cathodes in terms of safety and energy density. These materials are composites of a monoclinic layered phase Li$_2$MnO$_3$ integrated with a trigonal layered phase LiMO$_2$.[3,4] LMR-composites must, however, be charged to above 4.5 V to fully activate the Li$_2$MnO$_3$ component, and after activation the discharge capacity can reach 250 mAh/g at a C/10 rate.[3,5,6] The wide operating voltage (2.0–4.7 V) poses problems for the long-term cycling stability of the cells due to electrolyte decomposition and dissolution of transition metals, which occur at the electrode-electrolyte interface.[7,8] Another issue is the formation of a spinel like phase during cycling,[9] which can lead to uncontrolled voltage changes of the LMR-materials during their life span.[10,11] One of the approaches to strengthen the cathode interface against electrochemical and physical fatigue in the LIB cells is through surface modification.[12–14]

Recent works have demonstrated that surface modification using fluorine or phosphate wet chemistries[15–17] can reinforce the protection against electrode-electrolyte reactions, and facilitate charge transfer at the cathode surface, and hence improve the cycle life and rate performances of the cells.[6,15,16] Others

X. Zhang, I. Belharouak
Chemical Sciences and Engineering Division
Argonne National Laboratory
9700 S. Cass Ave, Argonne, IL 60439, USA
E-mail: belharouak@anl.gov
L. Li
School of Chemical Engineering and the Environment
Beijing Institute of Technology
Beijing 100081, China
Y. Lei, J. W. Elam
Energy System Division
Argonne National Laboratory
9700 S. Cass Ave, Argonne, IL 60439

A. Nie, R. S. Yassar
Department of Mechanical Engineering
Michigan Technological University
Houghton, MI 49931
X. Chen
Department of Mechanical Engineering
and NUANCE Center
Northwestern University
Evanston, IL 60208
R. L. Axelbaum
Department of Energy, Environmental and Chemical Engineering
Washington University in St. Louis
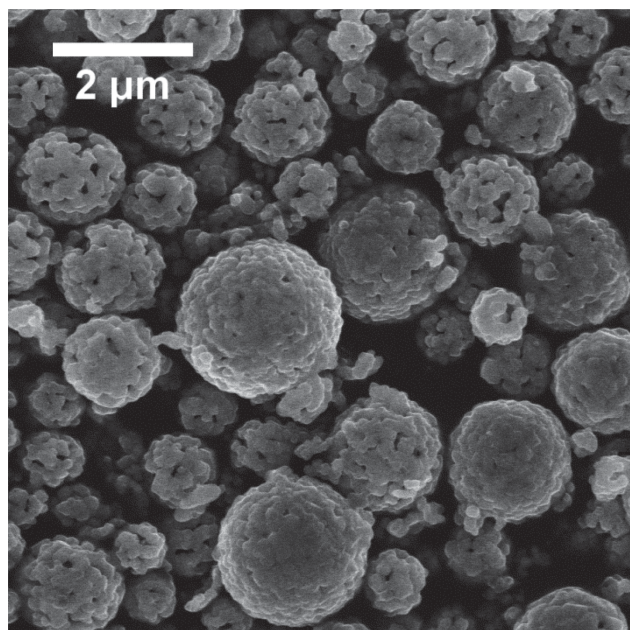One Brookings Dr., St. Louis, MO 63130, USA

FULL PAPER

Figure 1. SEM photograph of the porous $Li_{1.2}Ni_{0.13}Mn_{0.54}Co_{0.13}O_2$ particles for the ALD experiments.

have claimed a reduction in the irreversible capacity loss during the first activation cycle by using an Al_2O_3 coating.[18] Despite these improvements, wet chemistry processes are quite emperical in controlling film thickness, composition, uniformity and conformity of the coatings. On the other hand, atomic layer deposition (ALD) is a method to grow conformal ultrathin films with atomic layer thicknesses utilizing sequential and self-limiting surface chemical reactions.[14,19,20] ALD has been utilized to coat anode materials,[21–25] cathode materials,[26–30] and electrodes.[31–34] Electrochemical improvements had been reported in the case of Al_2O_3 coated $LiCoO_2$,[26,29,30,33] $LiNi_{1/3}Mn_{1/3}Co_{1/3}O_2$[28] and $Li_{1.2}Mn_{0.54}Ni_{0.13}Co_{0.13}O_2$.[30,34]

In this paper, we studied the electrochemical behavior of $Li_{1.2}Mn_{0.54}Ni_{0.13}Co_{0.13}O_2$ coated with Al_2O_3 and TiO_2 by an atomic layer deposition process. Lithium and graphite cells were made and electrochemical results were compared at room temperature (25 °C) and 55 °C with and without the coating. The morphology and chemical structure of the surface films were characterized by high-resolution transmission electron microscopy (HR-TEM) and X-ray photoemission spectroscopy (XPS).

2. Results and Discussion

2.1. Surface Characterization by HR-TEM/EDS

The substrate powder $Li_{1.2}Ni_{0.13}Mn_{0.54}Co_{0.13}O_2$ is spherical in shape and highly porous, as seen in **Figure 1**. The particles are poly-dispersed with a log-normal size distribution,[35] and the mean diameter is in the 2-3 μm range. $Li_{1.2}Ni_{0.13}Mn_{0.54}Co_{0.13}O_2$ adopts a typical layered-layered composite structure, as reported elsewhere.[3,36] In the ALD coated samples, neither Al_2O_3 nor

TiO_2 structures were detected by synchrotron X-ray powder diffraction (Figure S1), because the coating layers are composed of only tens of atomic layers and they can also be amorphous. HR-TEM and EDS were employed to elucidate the ultrathin surface film and analyze the elemental compositions of the ALD coated samples. **Figure 2**a is a HR-TEM image of a primary particle of the uncoated sample. Well-defined equidistant fringes in the bulk crystal confirm the layered structure of the bare $Li_{1.2}Ni_{0.13}Mn_{0.54}Co_{0.13}O_2$ material used in this study. The surface of the uncoated $Li_{1.2}Ni_{0.13}Mn_{0.54}Co_{0.13}O_2$ appears clean and smooth. In the bulk, distinct domains of different crystalline orientation (i.e., grains) can be observed in Figures 2a-c, indicating a polycrystalline structure of the primary particles. The Al_2O_3 and TiO_2 coated samples have identical layered fringes in the bulk; however, their surfaces are quite different morphologically (Figures 2b and c). The Al_2O_3 coated sample has a uniform and smooth coating, which is consistent with an amorphous, conformal ALD Al_2O_3 film (Figure 2b). The film is estimated to be 2~3 nm thick. Hence the growth rate of Al_2O_3 film was about 2~3 Å per ALD cycle, in agreement with reported data on $LiCoO_2$ and $LiMn_2O_4$ powders.[26,27] This ALD Al_2O_3 growth rate of 2-3 Å/cycle is about two times larger than the accepted growth rate of 1.2 Å/cycle observed on most surfaces,[19] and may indicate a CVD component resulting from the reaction of TMA with residual H_2O in the cathode powder. The TiO_2 coated sample surface appears to be discontinuous such that aggregated particles can be observed on the $Li_{1.2}Ni_{0.13}Mn_{0.54}Co_{0.13}O_2$ particle surface (blue arrow in Figure 2c). Thus, a well-defined boundary between the TiO_2 coating and the bulk is not evident. Moreover, no crystal fringe could be observed at the particle surface, hence the TiO_2 coating is likely amorphous as well. The TiO_2 thickness varies between 0 and 2 nm, with an average value below 1 nm. This value is consistent with the accepted growth rate for ALD TiO_2 prepared under these conditions.[37] The distinction between Al_2O_3 and TiO_2 ALD coatings can be ascribed to the difference in their preferential nucleation fashions. While ALD provides conformal coatings of Al_2O_3 thin films, TiO_2 prefers island-like growth. It forms small islands in the first ALD cycles which gradually merge and generates surface roughness, as reported by others.[37–39]

The elemental composition of the surface and bulk of $Li_{1.2}Ni_{0.13}Mn_{0.54}Co_{0.13}O_2$ particles was probed by local-point EDS, as indicated with black crosses in the corresponding HAADF-STEM images (Figures 2d-f). Since the image intensity (contrast) in a HAADF image is proportional to the atomic number (Z), Al_2O_3 and TiO_2 coatings have a very low contrast under this mode. The corresponding local-point STEM-EDS spectra were acquired for 1 min with a probe size less than 1 nm for more precise data acquisition. The uncoated material has identical elemental composition near the surface and in the bulk. All of the Mn, Ni and Co signals can be detected (Figure 2g). The Cu-K_α and Cu-K_β arose from the contribution of the TEM sample grid. The EDS spectra of the bulk of the Al_2O_3 and TiO_2 coated samples were also similar to that of the uncoated powder, where only the transition metals and oxygen were detected (Figures 2h-i). As the electron beam probed the edges of the coated powders, sharp Al-K_α and Ti-K_α signals emerged, confirming the presence of Al and Ti elements at the surfaces.

Materials
Views
www.MaterialsViews.com

ADVANCED
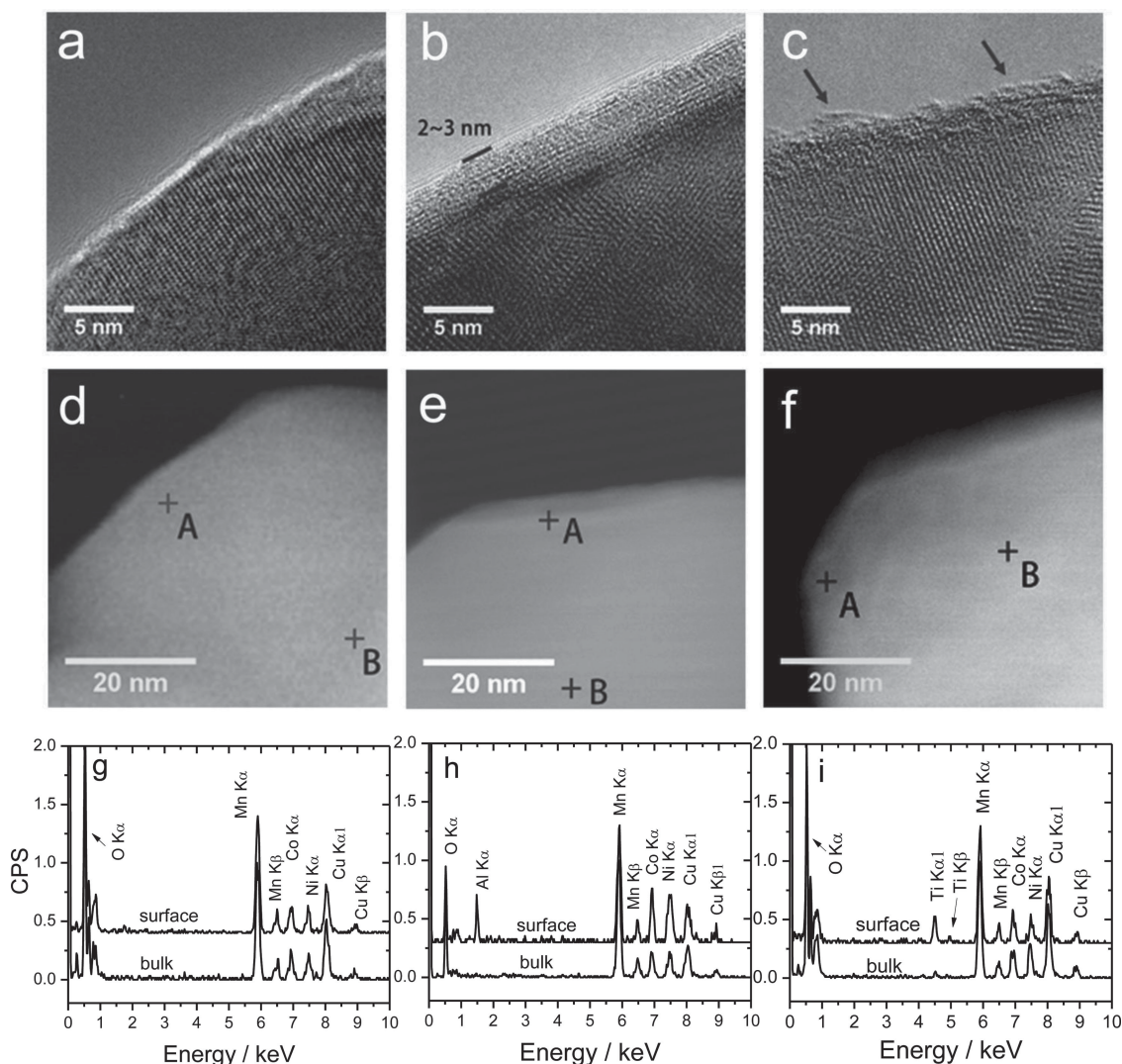ENERGY
MATERIALS
www.advenergymat.de

FULL PAPER

Figure 2. HR-TEM, HAADF photographs and EDS spectra of the uncoated (a, d and g), Al_2O_3 coated (b, e and h) and TiO_2 coated (c, f and i) $Li_{1.2}Ni_{0.13}Mn_{0.54}Co_{0.13}O_2$ particles by ALD.

2.2. XPS Analysis

With the confirmation of Al and Ti elements on the sample surfaces, XPS was used to probe the chemical structure of the species grown on the surfaces. In general, the high-resolution XPS spectra of the three powders all showed $2p_{1/2}$ and $2p_{3/2}$ core level peaks, belonging to the Mn, Co and Ni cations, as shown in **Figure 3**. However, the peaks for the powders with surface ALD coatings have weaker intensities than those of the uncoated powder, due to the lower weight ratios of the transition metals near the outermost surface. The Mn $2p_{3/2}$ peak fits well with a single peak with a binding energy (BE) of 642.7 eV, which is in a good agreement with Mn^{4+} ions in other manganese-based layered compounds.[40] The Co $2p_{3/2}$ has a binding energy of 780.8 eV which is very close to the reported BE of Co^{3+} (780 eV) in layered $LiMO_2$ (M = Ni, Co and Mn).[40–42] The two weak satellite peaks near 790 eV and 805 eV in the Co 2p spectra (Figure 3) are characteristic of a

Co^{3+} ion in an octahedral environment.[42] The Ni $2p_{3/2}$ XPS spectra for these samples have a BE of 855.7 eV, which is a value close enough to that of Ni^{3+} in bulk $LiNiO_2$ instead of Ni^{2+} (854 eV[40,41]), which is consistent with other reports on similar layered compounds.[40,41] One possible mechanism is that the excess Li-ions at the surface tend to occupy sites in the transition metal slab in the layered structure which can result in raising the oxidation state of Ni^{2+} to compensate the charges.[41] The ALD coating layers Al_2O_3 and TiO_2 are bridged to the $Li_{1.2}Ni_{0.13}Mn_{0.54}Co_{0.13}O_2$ substrate *via* an oxygen bond. The Al $2p_{3/2}$ core level XPS spectrum shows a binding energy of 74.2 eV for the Al_2O_3 coated powder (**Figure 4**a). Taking the O 1s peak (532.0 eV) into consideration (Figure 3f), the chemical composition of the surface coating is confirmed to be Al_2O_3.[26,43] After 10 potentiostatic cycles (0.04 mV.s^{-1} between 2.0 and 4.6 V), the BE of the Al $2p_{3/2}$ core level shows a marginal shift only (74.0 eV), indicating a stable Al_2O_3 surface film against the electrochemical charge and discharge. Liu et al.,
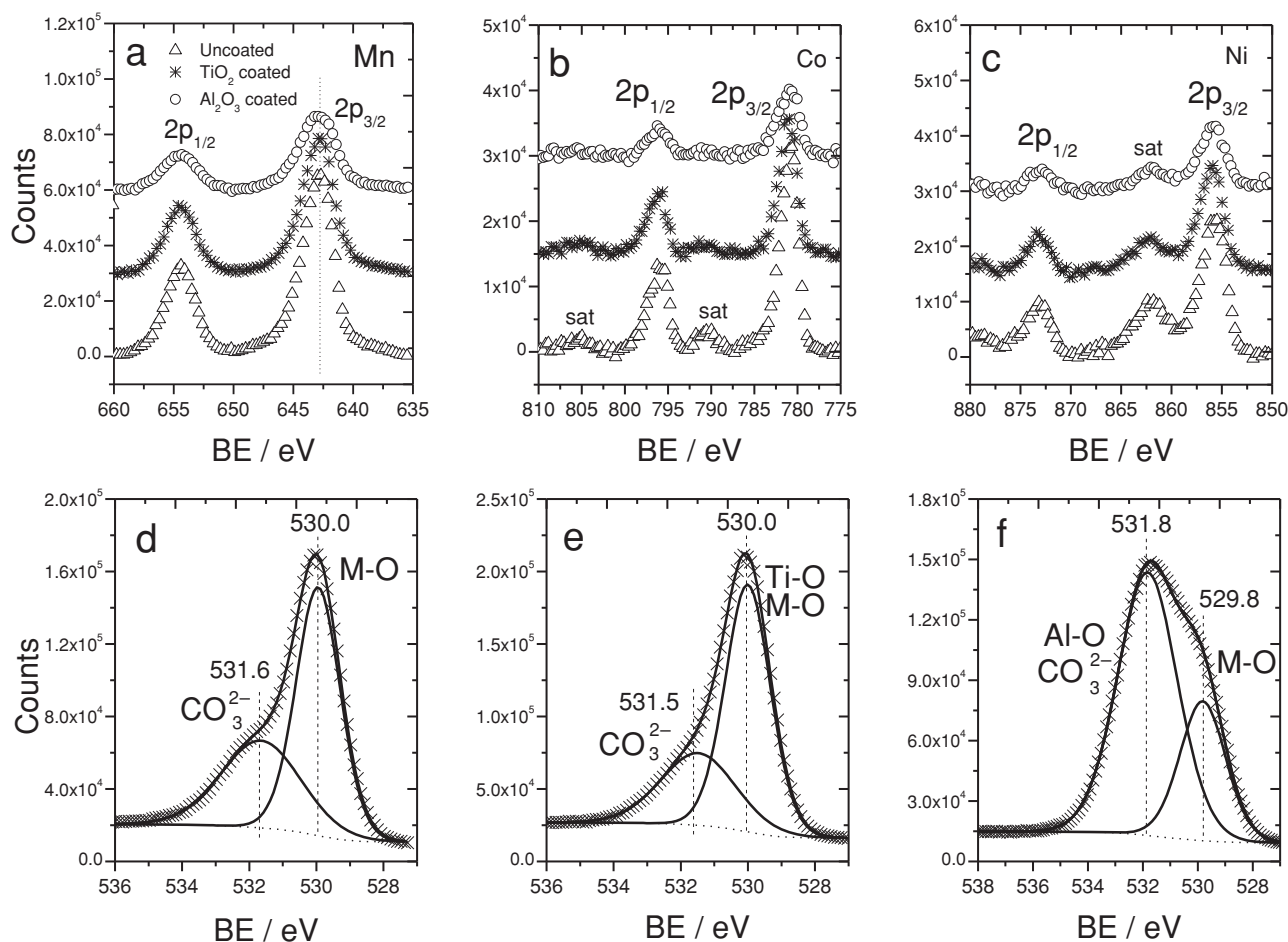
FULL PAPER

Figure 3. XPS core level spectra of transition metals and oxygen in uncoated, Al_2O_3 and TiO_2 coated $Li_{1.2}Ni_{0.13}Mn_{0.54}Co_{0.13}O_2$ powders: (a) Mn 2p; (b) Co 2p; (c) Ni 2p; (d) O 1s spectrum of the uncoated sample; (e) O 1s spectrum of the TiO_2 coated sample; (f) O 1s spectrum of the Al_2O_3 coated sample.

suggested that the Al_2O_3 film can be transformed into a stable Li-Al-O glass (or $LiAlO_2$) during lithiation,[33,44,45] which is inconsistent with our finding in this study.

The 2p core level binding energies of Ti are aligned at 458.7 eV ($2p_{3/2}$) and 464.4 eV ($2p_{1/2}$) (Figure 4b), and the corresponding O 1s peak has a BE of 530.0 eV (Figure 3e), which indicates the formation of TiO_2 on the particles surface.[30] After 10 potentiostatic cycles under the aforementioned test conditions, the XPS core level peaks of Ti display a degree of asymmetry, and can be deconvoluted into two $2p_{3/2}$ peaks at 458.9 eV and 457.9 eV, and two $2p_{1/2}$ peaks at 464.3 eV and 463.5 eV. The lower energy Ti $2p_{3/2}$ peak indicates the presence of Ti^{3+},[46,47] which could be attributed to Li_xTiO_2 generated in the electrochemical process following the reaction: $xLi + TiO_2 + xe^- \leftrightarrow Li_xTiO_2$.[48,49] The maximum insertion value x should be less than 0.5 in this voltage window,[48,49] which dictates the coexistence of Ti^{4+} and Ti^{3+} at the $Li_{1.2}Ni_{0.13}Mn_{0.54}Co_{0.13}O_2$ surface. This result clearly shows that the TiO_2 coating is participating in the redox reactions, which may cause degradation of the surface film after extensive cycling.[30]

2.3. Electrochemistry of the ALD Coated Materials

The uncoated and coated $Li_{1.2}Ni_{0.13}Mn_{0.54}Co_{0.13}O_2$ powders were tested in 2032 coin cells with Li-metal foil anodes. The overall shapes of the voltage profiles of the cells were identical for the initial activation cycle, which was performed at the C/10 rate (1C = 200 mAg^{-1}) between 2.0 and 4.8 V at 55 °C, as seen in **Figure 5**a. The voltage plateau observed at 4.5 V originates from the electrochemical activation of the Li_2MnO_3 component in the $Li_{1.2}Ni_{0.13}Mn_{0.54}Co_{0.13}O_2$.[5,50] The pristine and TiO_2 coated samples have identical voltage profiles with a discharge capacity of 300 and 310 mAhg^{-1}, respectively. A shoulder at the end-of-discharge of the TiO_2 coated material evolves between 2.0 and 2.5 V (Figure 5), which is a contribution from Li_xTiO_2 surface film.[48,49] As a consequence, the TiO_2 coated sample has a slightly higher discharge capacities and coulombic efficiency (87.6%) in the first cycle, compared to those of the uncoated sample (81.7%) and the Al_2O_3-coated sample (84.1%), as seen in **Table 1**. The Al_2O_3 coated sample, however, shows a higher over potential during the discharge (Figure 5) because of a higher charge transfer resistance across the conformal Al_2O_3
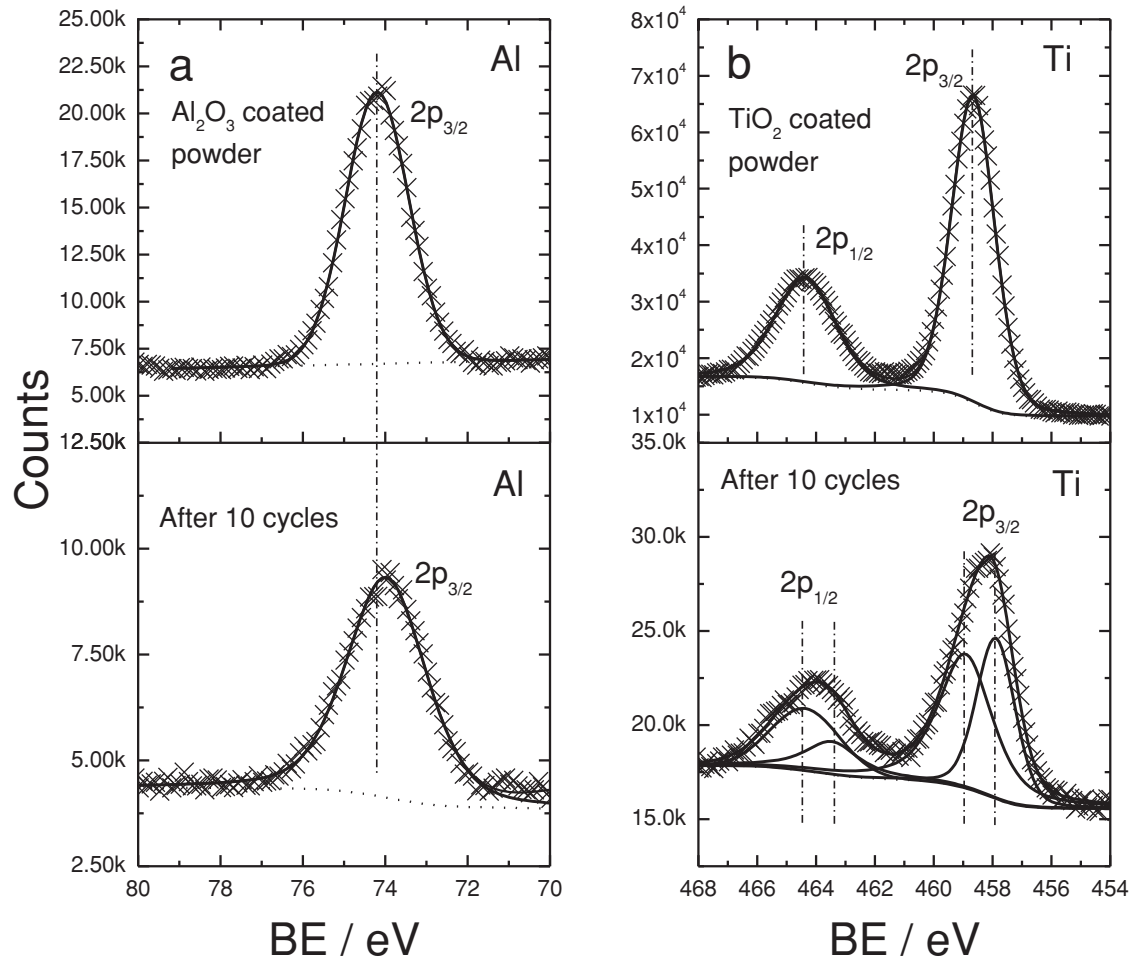
www.MaterialsViews.com

ADVANCED
ENERGY
MATERIALS
www.advenergymat.de

FULL PAPER

Figure 4. XPS core level spectra of Al 2p, and Ti 2p in uncoated, Al_2O_3 and TiO_2 coated $Li_{1.2}Ni_{0.13}Mn_{0.54}Co_{0.13}O_2$ powders by ALD before and after electrochemical cycling.
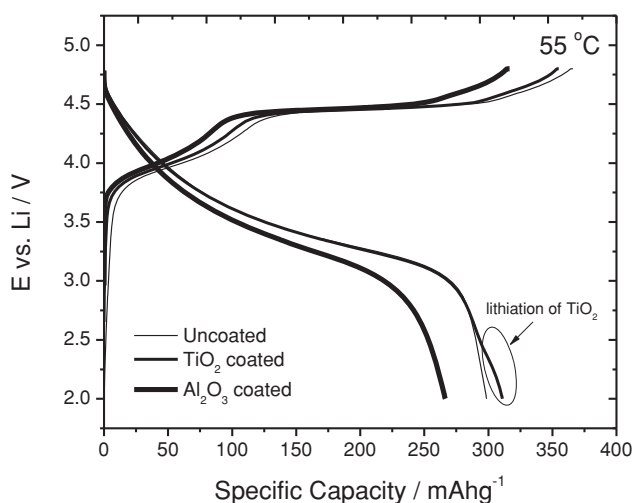

Figure 5. Voltage profiles of the $Li/Li_{1.2}Ni_{0.13}Mn_{0.54}Co_{0.13}O_2$ cells with Al_2O_3 and TiO_2 ALD coatings, which were tested at the C/10 rate between 2.0 and 4.8 V for the initial cycle. Testing temperature was 55 °C.

film (Figure 2S), which leads to a lower discharge capacity (266 mAhg^{-1}). Table 1 also indicates that the first cycle efficiencies of the ALD coated samples are only slightly affected by temperature, unlike the uncoated sample which shows a noticeable efficiency drop at 55 °C. This efficiency drop is most probably caused by an accelerated reactivity of the uncoated cathode material with the electrolyte at 55 °C.[51] These results allow us to safely conclude that the ALD surface coating can protect the cathode surface, making it more resilient to the HF attack and in general to parasitic reactions with electrolytes at high temperatures.

Cyclic voltammetry of $Li_{1.2}Ni_{0.13}Mn_{0.54}Co_{0.13}O_2$ and the ALD coated samples were conducted at a scan rate of 0.04 mV/s between open-circuit-voltage (OCV) and 4.8 V for the first cycle, followed by a 10 cycles conducted at the same scan rate between 2.0 and 4.6 V (**Figure 6**a, b and c). In general, the voltammograms of the uncoated sample and the ALD coated samples have shown similar curves in the first CV cycle, indicating the typical redox reactions of the transition metal cations occurring in $Li_{1.2}Ni_{0.13}Mn_{0.54}Co_{0.13}O_2$. The first anodic peak at

Table 1. Initial-cycle capacities and coulombic efficiencies of the Li/Li$_{1.2}$Ni$_{0.13}$Mn$_{0.54}$Co$_{0.13}$O$_2$ cells with Al$_2$O$_3$ and TiO$_2$ ALD coatings.

Samples	Test Temperature	1st Charge Capacity [mAhg^{-1}]	1st Discharge Capacity [mAhg^{-1}]	Efficiency [%]
Uncoated	RT	335	283	84.5
	55 °C	366	299	81.7
Al$_2$O$_3$ coated	RT	295	248	84.1
	55 °C	317	266	83.9
TiO$_2$ coated	RT	328	287	87.5
	55 °C	355	311	87.6

4.0 V is attributed to the Ni^{2+} and Co^{3+} cations being oxidized to the tetravalent states. The second anodic peak at 4.6 V is very pronounced, which arises from the electrochemical activation of Li$_2$MnO$_3$, as discussed earlier. The cathodic region is composed of a very broad peak including the Co^{4+}/Co^{3+}, Ni^{4+}/Ni^{2+} and Mn^{4+}/Mn^{3+} redox couples.[52] At the subsequent 5th and 10th CV cycles, the cathodic peak near 3.0 V evolved towards to a lower voltage and attenuated as cycle number increased. This feather indicates a rapid capacity fading and voltage decay of the uncoated Li$_{1.2}$Ni$_{0.13}$Mn$_{0.54}$Co$_{0.13}$O$_2$.

The CV of the TiO$_2$ and Al$_2$O$_3$ coated samples are almost identical to that of the bare sample for the 1st CV cycle, as seen in Figure 6b and 6c, respectively. A small cathodic peak can be observed between 2.0 and 2.4 V for TiO$_2$ coated sample (inset in Figure 6b), which is due to the slow lithiation of TiO$_2$ to form Li$_x$TiO$_2$ at the surface, as discussed earlier. Interestingly, the electrochemical activation of the Li$_2$MnO$_3$-like phase in Li$_{1.2}$Ni$_{0.13}$Mn$_{0.54}$Co$_{0.13}$O$_2$ was not noticeably affected by ALD surface coating, as the position of the anodic peaks observed beyond 4.5 V for both coated samples did not change, which is indicative of no change in the oxygen activity after coating (Figure 5). Additionally, no obvious decay of voltage and capacity can be observed after the 1st activation cycle for these coated samples (Figure 6b and 6c). Therefore, it is anticipated that the ALD surface coating may reduce voltage decay and capacity fading at a low scan rate and room temperature.

The cycling performances of lithium cells comprising the pristine and ALD coated samples are shown in **Figure 7**a (RT) and in Figure 7b (55 °C), respectively. The first three cycles are formation cycles performed at the C/10 rate to fully activate Li$_{1.2}$Ni$_{0.13}$Mn$_{0.54}$Co$_{0.13}$O$_2$ and also to form a stable passivation layer. Thereafter, the current density was elevated to C/3 rate for 50 cycles. At room temperature, Li$_{1.2}$Ni$_{0.13}$Mn$_{0.54}$Co$_{0.13}$O$_2$ exhibited a 32% capacity fade from 220 at the 4th cycle to 150 mAhg^{-1} after 50 cycles. The ALD coated samples showed lower capacity fade with cycling, i.e. 18% and 22% for the Al$_2$O$_3$ and TiO$_2$ coatings, respectively. However, when the testing temperature was increased to 55 °C, the TiO$_2$ coated sample exhibited a poor capacity retention (70%), which was translated by a capacity decline from 240 to 170 mAhg^{-1} (Figure 7b). Under these conditions, the cycling behavior of the TiO$_2$ coated sample was quite similar to that of the bare sample. Thus, the nonconformal TiO$_2$ surface film
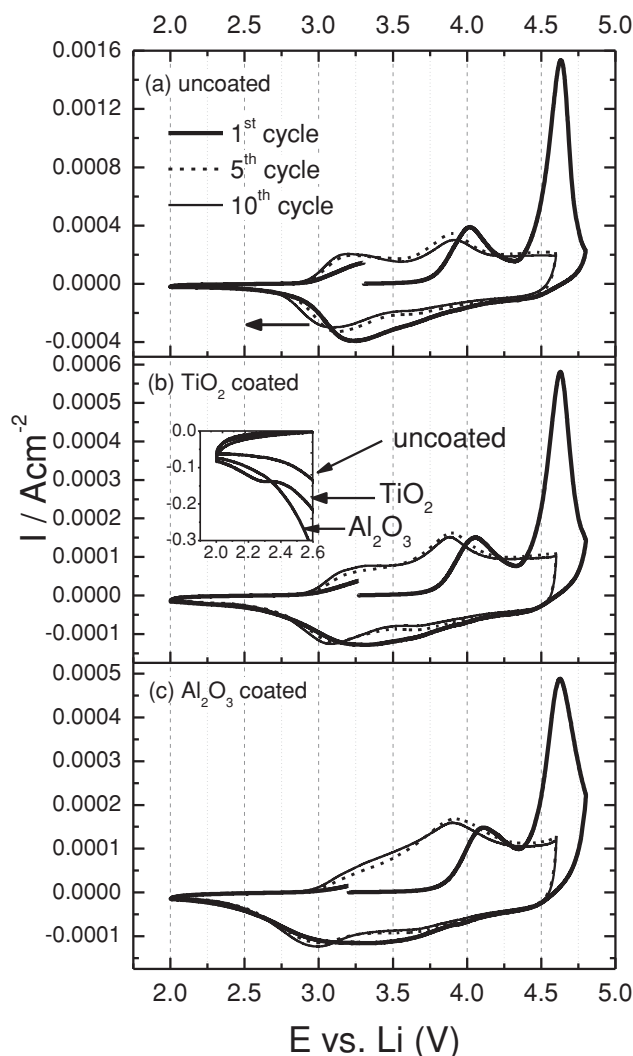

Figure 6. Cyclic voltammetry of the Li/Li$_{1.2}$Ni$_{0.13}$Mn$_{0.54}$Co$_{0.13}$O$_2$ cells with Al$_2$O$_3$ and TiO$_2$ ALD coatings, which is tested at a scan rate of 0.04 mV/s between 2.0 and 4.8 or 4.6 V, conducted at the room temperature.

which undergoes redox reactions during charge and discharge had no positive impact on the cycling stability of Li$_{1.2}$Ni$_{0.13}$Mn$_{0.54}$Co$_{0.13}$O$_2$ at 55 °C. The conformal Al$_2$O$_3$ coating, however, provided superior cycling stability compared to non-coated sample at both room temperature and 55 °C in the lithium cells. The differences between these coatings can be attributed mainly to the conformity and reactivity behaviors of the surface films upon charge and discharge, if we keep in mind that the thicknesses of these films were quite similar. Unlike the ALD-Al$_2$O$_3$ coating, the TiO$_2$ one was not uniform enough to protect the particles against electrolyte reactions, and it also contributed to the redox reactions which probably led to additional catalytic reactions that accelerated the loss of the surface protection.[53]

The ALD coatings, however, have less significance with respect to the behavior of the materials when cycled in cells containing graphite anodes, such as MCMB in our case (**Figure 8**a and 8b). Though slight improvements are seen in
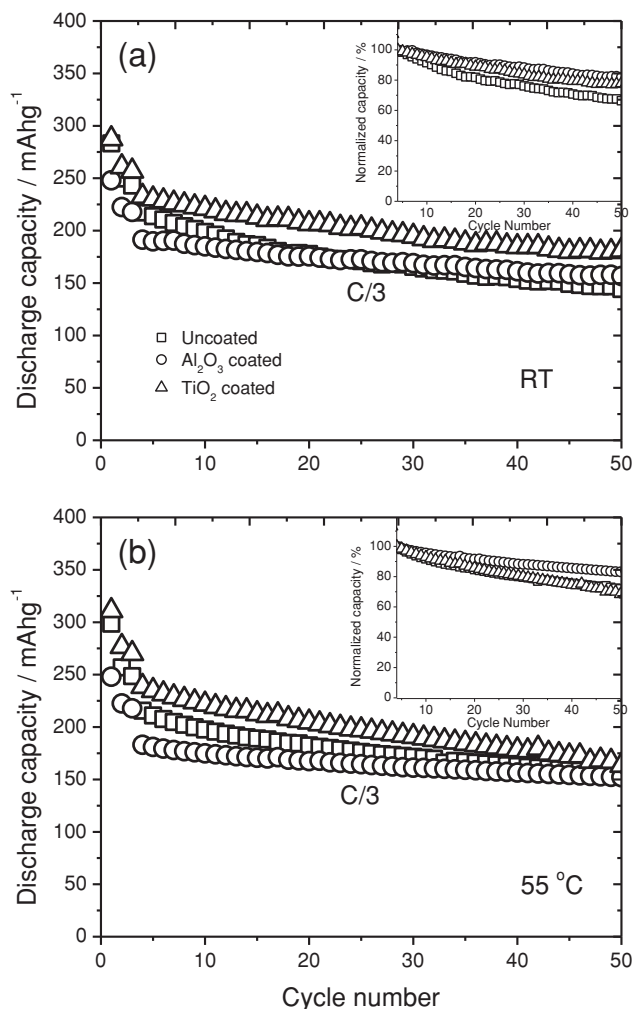
Figure 7. Cycling performance of the $Li/Li_{1.2}Ni_{0.13}Mn_{0.54}Co_{0.13}O_2$ cells with Al_2O_3 and TiO_2 ALD coatings, conducted at (a) room temperature and (b) 55 °C. Test procedure: cycle 1 at C/10 rate between 2.0 and 4.8 V for activation; cycle 2-3 is formation cycle at C/10 between 2.0 and 4.6 V; cycle 4–50 at C/3 between 2.0 and 4.6 V. The inset figures are normalized capacity retention at C/3 rate.

Figure 8. Cycling performance of the $MCMB/Li_{1.2}Ni_{0.13}Mn_{0.54}Co_{0.13}O_2$ with TiO_2 and Al_2O_3 ALD coatings, conducted at (a) room temperature and (b) 55 °C. Test procedure: cycle 1 at C/10 rate between 2.0 and 4.8 V for activation; cycle 2-3 is formation cycle at C/10 between 2.0 and 4.5 V; cycle 4–50 at C/3 between 2.0 and 4.5 V. The inset figures are normalized capacity retention at C/3 rate.

the cycling of the graphite-cell at room temperature for both coatings compared to the pristine sample (inset in Figure 8a), the three samples, including the best performing one (ALD-Al_2O_3 sample), exhibited quite similar cycling behavior at 55 °C (inset in Figure 8b). This result clearly shows that the effectiveness of the ALD coating at room temperature can be jeopardized at 55 °C in practical cells. In this case, the capacity fade is mainly due the continuous growth of the solid electrolyte interface (SEI) on the anode, which increases the cell impedance and consequently worsens the kinetics and capacity with cycling.[54,55] A similar observation has been found in the case of AlF_3 coating when $Li_{1.1}(Ni_{0.15}Co_{0.1}Mn_{0.55})O_{1.95}$ was cycled against graphite.[17] Therefore, we suggest that when results are reported on the effectiveness of coatings in lithium cells, it would always be helpful to identify the impact of these coating in practical Li-ion battery configurations, especially at elevated temperatures.
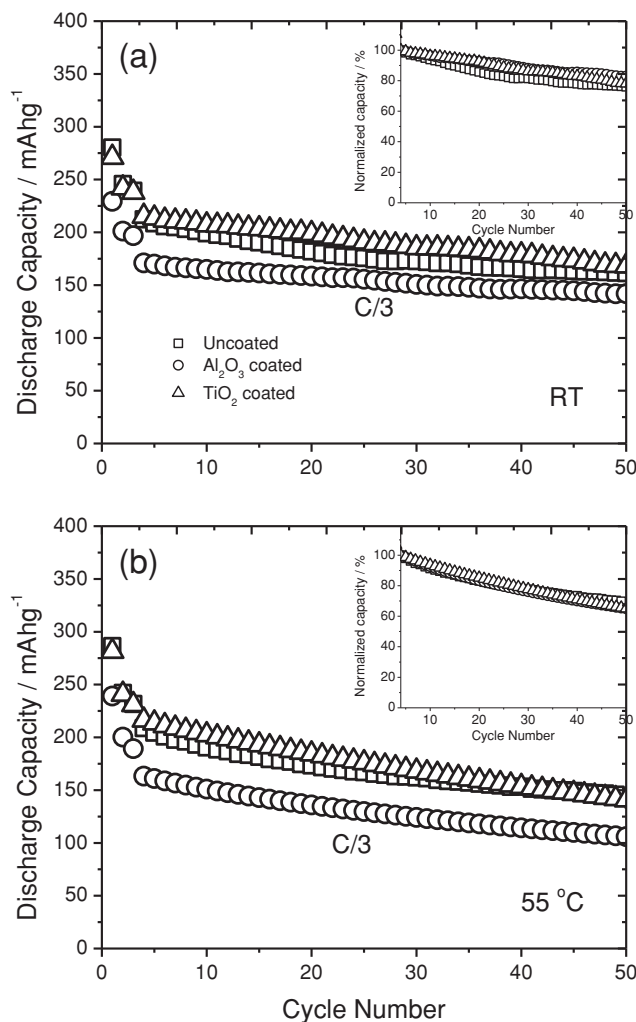
3. Conclusion

The ALD technique was applied to coat $Li_{1.2}Ni_{0.13}Mn_{0.54}Co_{0.13}O_2$ porous powder with ultrathin Al_2O_3 and TiO_2 films. These ALD coatings have two distinguished surface morphologies, of which the Al_2O_3 surface film showed great uniformity and conformity, while the coated TiO_2 film appeared as nanoparticles at the surface, as seen by HR-TEM. The cycling behaviors of cells comprising the pristine and ALD coated powders as cathodes, and Li or MCMB as anodes, were evaluated at the room temperature and 55 °C at the C/3 rate. In the lithium cells tested at room temperature, higher first cycle coulombic efficiencies and improved cycling were attained for the ALD coated samples, which can be directly attributed to the protective role of the surface films against electrode-electrolyte reactions at the high voltage. XPS measurements demonstrated that these coatings

FULL PAPER

remain at the cathode interface after extensive charge and discharge. The TiO$_2$ coating, however, suffered from a transformation to Li$_x$TiO$_2$ upon lithiation leading to the emergence of Ti^{3+} surface cations, which are likely responsible for catalysis reactions that exacerbate the capacity fading, especially at 55 °C. Overall, the ALD-Al$_2$O$_3$ coating demonstrated better surface protection for the cathode powder and thus better cycling stability compared to TiO$_2$. However, the cells comprising the ALD coated samples and MCMB anode did not show a noticeable improved cycling stability, possibly due to the instability of the anode. In our opinion, it is important to improve the electrochemical stability of graphite as well, *e.g.*, by a surface modification method, so that the overall performance improvement of the LIB cells can be preserved.

4. Experimental Section

Materials Synthesis and ALD Coating: The composite material Li$_{1.2}$Ni$_{0.13}$Mn$_{0.54}$Co$_{0.13}$O$_2$ was synthesized using a spray pyrolysis process, as described earlier.[35] The reagents for the composite material synthesis are lithium nitrate anhydrous (LiNO$_3$), nickel nitrate hexahydrate (Ni(NO$_3$)$_2$·6H$_2$O), cobalt nitrate hexahydrate (Co(NO$_3$)$_2$·6H$_2$O) and manganese nitrate tetrahydrate (Mn(NO$_3$)$_2$·4H$_2$O) from Sigma Aldrich. The Li$_{1.2}$Ni$_{0.13}$Mn$_{0.54}$Co$_{0.13}$O$_2$ powder from the spray pyrolysis reactor was post-annealed at 850 °C for 2 hours. Ultrathin Al$_2$O$_3$ and TiO$_2$ films were prepared respectively over Li$_{1.2}$Ni$_{0.13}$Mn$_{0.54}$Co$_{0.13}$O$_2$ powder surface in a continuous-flow ALD reactor operated under a base pressure of ~1 Torr.[56] Typically, 500 mg of substrate powders were well-spread in a flat stainless steel tray and loaded into the ALD reaction chamber. An Al$_2$O$_3$ thin films were deposited using 10 ALD cycles of trimethylaluminum (TMA) and H$_2$O at 150 °C. TiO$_2$ was prepared using 20 ALD cycles of titanium isopropoxide (TTIP) and H$_2$O at 150 °C. The precursor dose and purge time were 30 seconds and 60 seconds, respectively.

Material Characterization: X-ray powder diffraction (XRD) results of the composite powders before and after ALD coating were obtained using a synchrotron high-energy X-ray beam (115 keV) with a wavelength of 0.108 Å at the beamline 11-ID-C at the Advanced Photon Source (APS) at Argonne National Laboratory. The TEM characterization was conducted on an aberration-corrected JEOL JEM-ARM200CF scanning transmission electron microscope (STEM) equipped with a 200 keV Schottky cold-field emission gun, a high-angle annular dark field (HAADF) detector, and an annular bright field (ABF) detector. The elemental analysis was performed using point energy dispersive spectrometer (EDS) spectrum under STEM mode for a better resolution. Here, a 22-mrad-probe convergence angle was used for all the images and spectra acquisition.

The surface chemistry of the uncoated and ALD coated powders and cycled electrodes were analyzed using X-ray photoelectron spectroscopy (XPS, Thermo Scientific ESCALAB 250Xi) with Al Kα radiation (1486.7 eV). The XPS spectra were collected in constant analyzer energy (CAE) mode at a 50.0 eV pass energy and 500 μm spot size. The binding energies (BE) of the samples were calibrated using the adventitious C 1s peak (BE = 284.8 eV). Prior to the XPS analysis, all the powder samples were dried under vacuum overnight to reduce the amount of the surface-absorbed contaminant species. The electrodes for ex-situ XPS analysis were rinsed by dimethyl carbonate (DMC) to wash off the residual electrolyte in the electrodes, which were further subjected to drying under vacuum at 60 °C for 6 hours. The XPS spectra were deconvoluted using a public software XPSPeak4.1 using Lorentzian-Gaussian fitting with a Shirley-type background.

Electrochemical Analysis: The electrochemistry of the composite materials was studied using 2032 coin cells. The ratio of active material Li$_{1.2}$Ni$_{0.13}$Mn$_{0.54}$Co$_{0.13}$O$_2$, SFG-6 graphite, Super-P conductive carbon and polyvinylidene (PVdF 1120, Kureha Corp.) was 80:5:5:10 by weight in the positive electrodes. The electrode disc was 1.6 cm in diameter and had an active material loading of *c.a.* 2.9 mg/cm^2. The negative electrodes

were Li foil or meso-carbon-micro-bead (MCMB). A 1.2 M solution of LiPF$_6$ in ethylene carbonate/ethyl methyl carbonate (EC:EMC = 3:7 by volume, Tomiyama) was used as the electrolyte. The positive and negative electrodes were separated by a micro-porous trilayer membrane separator (PP/PE/PP, Celgard 2325). The cyclic voltammetry (CV) and electrochemical impedance spectroscopy (EIS) data were obtained using a Solartron 1470E multichannel potentiostat/cell test system coupled with Solartron 1400 FRA Impedance analyzer.

Supporting Information

Supporting Information is available from the Wiley Online Library or from the author.

[1] Y. K. Sun, S. T. Myung, B. C. Park, J. Prakash, I. Belharouak, K. Amine, *Nat. Mater.* **2009**, *8*, 320–324.

[2] J. B. Goodenough, K. S. Park, *J. Am. Chem. Soc.* **2013**, *135*, 1167–1176.

[3] M. M. Thackeray, S. H. Kang, C. S. Johnson, J. T. Vaughey, R. Benedek, S. A. Hackney, *J. Mater. Chem.* **2007**, *17*, 3112–3125.

[4] J. H. Lim, H. Bang, K. S. Lee, K. Amine, Y. K. Sun, *J. Power Sources* **2009**, *189*, 571–575.

[5] C. S. Johnson, J. S. Kim, C. Lefief, N. Li, J. T. Vaughey, M. M. Thackeray, *Electrochem. Commun.* **2004**, *6*, 1085–1091.

[6] S. H. Kang, M. M. Thackeray, *Electrochem. Commun.* **2009**, *11*, 748–751.

[7] D. Aurbach, Y. Talyosef, B. Markovsky, E. Markevich, E. Zinigrad, L. Asraf, J. S. Gnanaraj, H. J. Kim, *Electrochim. Acta* **2004**, *50*, 247–254.

[8] M. Jiang, B. Key, Y. S. Meng, C. P. Grey, *Chem. Mater.* **2009**, *21*, 2733–2745.

[9] B. Xu, C. R. Fell, M. F. Chi, Y. S. Meng, *Energy Environ. Sci.* **2011**, *4*, 2223–2233.

[10] A. Ito, K. Shoda, Y. Sato, M. Hatano, H. Horie, Y. Ohsawa, *J. Power Sources* **2011**, *196*, 4785–4790.

[11] M. Gu, I. Belharouak, J. M. Zheng, H. M. Wu, J. Xiao, A. Genc, K. Amine, S. Thevuthasan, D. R. Baer, J. G. Zhang, N. D. Browning, J. Liu, C. M. Wang, *ACS Nano* **2013**, *7*, 760–767.

Materials
Views
www.MaterialsViews.com

ADVANCED
ENERGY
MATERIALS
www.advenergymat.de

FULL PAPER

[12] Z. H. Chen, Y. Qin, K. Amine, Y. K. Sun, *J. Mater. Chem.* **2010**, *20*, 7606–7612.

[13] S. T. Myung, K. Amine, Y. K. Sun, *J. Mater. Chem.* **2010**, *20*, 7074–7095.

[14] X. B. Meng, X. Q. Yang, X. L. Sun, *Adv. Mater.* **2012**, *24*, 3589–3615.

[15] S. H. Kang, C. S. Johnson, J. T. Vaughey, K. Amine, M. M. Thackeray, *J. Electrochem. Soc.* **2006**, *153*, A1186–A1192.

[16] S. H. Kang, M. M. Thackeray, *J. Electrochem. Soc.* **2008**, *155*, A269–A275.

[17] H. Deng, I. Belharouak, C. S. Yoon, Y. K. Sun, K. Amine, *J. Electrochem. Soc.* **2010**, *157*, A1035–A1039.

[18] Q. Y. Wang, J. Liu, A. V. Murugan, A. Manthiram, *J. Mater. Chem.* **2009**, *19*, 4965–4972.

[19] S. M. George, *Chem. Rev.* **2010**, *110*, 111–131.

[20] J. W. Elam, N. P. Dasgupta, F. B. Prinz, *Mrs Bulletin* **2011**, *36*, 899–906.

[21] M. Q. Snyder, S. Trebukhova, B. Ravdel, M. C. Wheeler, J. DiCarlo, C. P. Tripp, W. J. DeSisto, *Solid-State Ionics* **2006**, *972*, 331–338.

[22] M. Q. Snyder, S. A. Trebukhova, B. Ravdel, M. C. Wheeler, J. DiCarlo, C. P. Tripp, W. J. DeSisto, *J. Power Sources* **2007**, *165*, 379–385.

[23] L. A. Riley, A. S. Cavanagh, S. M. George, Y. S. Jung, Y. F. Yan, S. H. Lee, A. C. Dillon, *ChemPhysChem* **2010**, *11*, 2124–2130.

[24] I. Lahiri, S. M. Oh, J. Y. Hwang, C. Kang, M. Choi, H. Jeon, R. Banerjee, Y. K. Sun, W. Choi, *J. Mater. Chem.* **2011**, *21*, 13621–13626.

[25] X. F. Li, X. B. Meng, J. Liu, D. S. Geng, Y. Zhang, M. N. Banis, Y. L. Li, J. L. Yang, R. Y. Li, X. L. Sun, M. Cai, M. W. Verbrugge, *Adv. Funct. Mater.* **2012**, *22*, 1647–1654.

[26] Y. S. Jung, A. S. Cavanagh, A. C. Dillon, M. D. Groner, S. M. George, S. H. Lee, *J. Electrochem. Soc.* **2010**, *157*, A75-A81.

[27] D. S. Guan, J. A. Jeevarajan, Y. Wang, *Nanoscale* **2011**, *3*, 1465–1469.

[28] L. A. Riley, S. Van Ana, A. S. Cavanagh, Y. F. Yan, S. M. George, P. Liu, A. C. Dillon, S. H. Lee, *J. Power Sources* **2011**, *196*, 3317–3324.

[29] I. D. Scott, Y. S. Jung, A. S. Cavanagh, Y. F. An, A. C. Dillon, S. M. George, S. H. Lee, *Nano Lett.* **2011**, *11*, 414–418.

[30] H. M. Cheng, F. M. Wang, J. P. Chu, R. Santhanam, J. Rick, S. C. Lo, *J. Phys. Chem. C* **2012**, *116*, 7629–7637.

[31] Y. S. Jung, A. S. Cavanagh, L. A. Riley, S. H. Kang, A. C. Dillon, M. D. Groner, S. M. George, S. H. Lee, *Adv. Mater.* **2010**, *22*, 2172–2176.

[32] L. A. Riley, A. S. Cavanagh, S. M. George, S. H. Lee, A. C. Dillon, *Electrochem. Solid-State Lett.* **2011**, *14*, A29–A31.

[33] Y. S. Jung, P. Lu, A. S. Cavanagh, C. Ban, G. H. Kim, S. H. Lee, S. M. George, S. J. Harris, A. C. Dillon, *Adv. Energy. Mater.* **2012**, *3*, 213–219.

[34] Y. S. Jung, A. S. Cavanagh, Y. F. Yan, S. M. George, A. Manthiram, *J. Electrochem. Soc.* **2011**, *158*, A1298–A1302.

[35] X. F. Zhang, R. L. Axelbaum, *J. Electrochem. Soc.* **2012**, *159*, A834–A842.

[36] J. Bareno, M. Balasubramanian, S. H. Kang, J. G. Wen, C. H. Lei, S. V. Pol, I. Petrov, D. P. Abraham, *Chem. Mater.* **2011**, *23*, 2039–2050.

[37] M. Ritala, M. Leskela, L. Niinisto, P. Haussalo, *Chem. Mater.* **1993**, *5*, 1174–1181.

[38] M. Ritala, M. Leskela, L. Niinisto, T. Prohaska, G. Friedbacher, M. Grasserbauer, *Thin Solid Films* **1994**, *249*, 155–162.

[39] V. Sammelselg, A. Rosental, A. Tarre, L. Niinisto, K. Heiskanen, K. Ilmonen, L. S. Johansson, T. Uustare, *Appl. Surf. Sci.* **1998**, *134*, 78–86.

[40] K. M. Shaju, G. V. S. Rao, B. V. R. Chowdari, *Electrochim. Acta* **2002**, *48*, 145–151.

[41] N. Tran, L. Croguennec, C. Labrugere, C. Jorde, P. Biensan, C. Delmas, *J. Electrochem. Soc.* **2006**, *153*, A261–A269.

[42] A. W. Moses, H. G. G. Flores, J. G. Kim, M. A. Langell, *Appl. Surf. Sci.* **2007**, *253*, 4782–4791.

[43] S. C. Ha, E. Choi, S. H. Kim, J. S. Roh, *Thin Solid Films* **2005**, *476*, 252–257.

[44] Y. Liu, N. S. Hudak, D. L. Huber, S. J. Limmer, J. P. Sullivan, J. Y. Huang, *Nano Lett.* **2011**, *11*, 4188–4194.

[45] A. T. Appapillai, A. N. Mansour, J. Cho, Y. Shao-Horn, *Chem. Mater.* **2007**, *19*, 5748–5757.

[46] C. M. Greenlief, J. M. White, C. S. Ko, R. J. Gorte, *J. Phys. Chem.* **1985**, *89*, 5025–5028.

[47] V. V. Atuchin, V. G. Kesler, N. V. Pervukhina, Z. Zhang, *J. Electron Spectrosc. Rel. Phenom.* **2006**, *152*, 18–24.

[48] F. Leroux, P. J. Dewar, M. Intissar, G. Ouvrard, L. F. Nazar, *J. Mater. Chem.* **2002**, *12*, 3245–3253.

[49] M. Wagemaker, W. J. H. Borghols, F. M. Mulder, *J. Am. Chem. Soc.* **2007**, *129*, 4323–4327.

[50] A. D. Robertson, P. G. Bruce, *Electrochem. Solid-State Lett.* **2004**, *7*, A294–A298.

[51] K. Araki, N. Sato, *J. Power Sources* **2003**, *124*, 124–132.

[52] C. S. Johnson, N. C. Li, C. Lefief, J. T. Vaughey, M. M. Thackeray, *Chem. Mater.* **2008**, *20*, 6095–6106.

[53] I. Belharouak, G. M. Koenig, T. Tan, H. Yumoto, N. Ota, K. Amine, *J. Electrochem. Soc.* **2012**, *159*, A1165–A1170.

[54] C. S. Wang, A. J. Appleby, F. E. Little, *J. Electroanal. Chem.* **2001**, *497*, 33–46.

[55] M. S. Wu, P. C. J. Chiang, J. C. Lin, *J. Electrochem. Soc.* **2005**, *152*, A1041–A1046.

[56] J. W. Elam, M. D. Groner, S. M. George, *Rev. Sci. Instrum.* **2002**, *73*, 2981–2987.